Solvent-free cross aldol condensation of aldehydes and ketones over $SrMo_{1-x}Ni_xO_{3-\delta}$ perovskite nanocrystals as heterogeneous catalysts

Lebohang Kekana , Ndzondelelo Bingwa [*]

Research Centre for Synthesis and Catalysis, Department of Chemical Sciences, University of Johannesburg, PO Box 542, Auckland Park, 2006, Johannesburg, South Africa

A B S T R A C T

Aldol condensation is arguably one of the most fascinating reactions that leads to the formation of C–C bonds. Its use in the pharmaceutical industry to synthesis complex drugs from simple aldehydes and ketones has become of paramount importance. Although this is one reaction that has lured a lot of attention, not enough has been explored in heterogeneous catalysis. In this work we have successfully synthesized multicationic perovskites *via* the soft-template method and characterized them thoroughly. The synthesized perovskite nanocrystals were found to have small S_{BET} however their catalytic application in the conversion of benzaldehyde (BAL) in the aldol condensation with diethyl ketone (DEK) was found to be astonishing. The synthesis was confirmed using many techniques, from determining the oxidation states of the materials using XPS. This gave access to determine the coordination of the metals in the perovskite lattice and also qualitatively assess the oxygen environments that exist. The oxygen vacancies and S_{BET} were used to assess the activity of the perovskite catalysts in the cross-aldol condensation reaction. The optimal conditions for this aldol condensation were found to be 120 °C after 25 h with no solvent using $SrMo_{0.5}Ni_{0.5}O_{3-\delta}$ inorganic perovskite which had the highest amount of oxygen vacant sites which gave a conversion of 88 % and an 82 % selectivity towards the desired cross-aldol condensation product. The use of dimethylformamide (DMF) for this reaction is discouraged as it reacts with BAL to produce a higher amide.

1. Introduction

A distinctive feature of oxide-type perovskite in catalysis is that they are fairly stable, and its properties can be tuned to fit a desired catalytic reaction. Perovskites are metal oxides with a structural formula, ABO_3, (A is a rare/alkaline earth metal and B is a transition metal), adopted from the first perovskite to be discovered, $CaTiO_3$ [1–3]. They are ideally cubic; however, other geometric deviations have been reported [4,5]. The tuning of perovskites to give an anticipated outcome can be achieved creating some distortions in the crystal geometry of the perovskite. The distortions can be brought about by cationic partial displacement, in which the cations are of different ionic radii. This will inherently influence the electronic structure, metal-oxygen bond, the metal-metal bond and it will produce sites that are cationic and anionic vacant [6]. An effect on these properties will affect the performance of the metal oxide.

Of the many reactions that result in the formation of the carbon-carbon bond, aldol condensation still proves itself to be one that can be used with bio-molecules as it utilizes compounds that are carbonyl-containing to produce an α,β-unsaturated ketone [7,8]. Since its discovery by Charles Wurtz in 1972, there have been some modifications of the aldol condensation reaction, *viz* Knoevenagel, Perkin, Diekmann and Henry [9–12]. Traditionally, these require the use of a homogeneous strong and active base catalyst that will aid in the abstraction of an α-proton on the carbonyl to generate an active enolate species which will consequently produce the desired aldol product [13,14]. The bases that are currently being used for the aldol condensation reaction are corrosive and some even harmful to our health. Moreover, they are in homogeneous solution, which makes them hard to recycle. Heterogeneous metal oxide catalysts, such as metals supported on modified silica [15–20], hydrotalcite [15], zeolites [21] and other metal oxides [22–24], however, the require addition of a co-catalyst and/or scavenger molecules, they are done at high temperatures, and they also require a hefty amount of time to run to completion [25–28].

The transformation of simple organic molecules to complex chemicals by formation of a new carbon-carbon bond has become one of the most fascinating events among researchers in the field drug discovery and synthesis [29–31]. This reaction can be used for the synthesizing long-chain alkane precursors [32–35].

Herein we report on the use of use of solid perovskite, $SrMo_{1-x}Ni_xO_{3-\delta}$ catalysts as active catalysts for the transformation of benzaldehyde and diethyl ketone to produce an asymmetric aldol product. This work investigates the electronic properties of the perovskite catalysts and their influence on the aldol condensation of benzaldehyde (BAL) with diethyl ketone (DEK). Furthermore, this study also showcases the plausibility of perovskites as driving catalysts for aldol condensation reaction.

2. Experimental

2.1. Materials

Poly(ethylene glycol)-*block* poly(propylene glycol)-*block*-poly(ethylene glycol) (Pluronic P-123 gel, 97 %), ammonia molybdate tetrahydrate $((NH_3)_6Mo_7O_{27}\bullet4H_2O$, 83 %), nitric acid ($HNO_3$, 70 %), and ethanol ($CH_3CH_2OH$, >97 %) were all procured from Sigma-Aldrich, while *n*-butanol was obtained from Associated Chemical Enterprise (C_4H_9OH, >99 %). Nickel(II) nitrate hexahydrate (Ni $(NO_3)_2\bullet6H_2O$, 99 %) was purchased from SRL chemicals while anhydrous strontium nitrate ($Sr(NO_3)_2$, 99 %) was obtained from BDH chemicals. The subtrate benzaldehyde (C_6H_5CHO, BAL, >99 %), the internal standards, octane (C_8H_{10}, >99 %) an *n*-decane ($C_{10}H_{22}$, >99 %), and dimethylformamide (C_2H_6NCHO, DMF, >98 %) were purchased from Sigma-Aldrich. Diethyl ketone ($C_4H_{10}CO$, DEK, >99 %), 1,3-dioxane (C_4H_8O) and tetrahydrofuran (C_4H_8O, THF) were acquired from SRL Chemicals.

2.2. Synthesis and characterization of the multicationic $SrMo_{1-x}Ni_xO_{3-\delta}$ inorganic perovskites

The synthesis of the multicationic inorganic $SrMo_xNi_xO_{3-\delta}$ was carried out using the soft-template method using the 0 g of Pluronic P-123 gel as the soft-template. The Pluronic P-123 gel was dissolved in 100 mL of *n*-butanol. In the solution of *n*-butanol and Pluronic P-123 gel, stoichiometric amounts of the metal nitrate salt precursors, $Sr(NO_3)_2$, $Ni(NO_3)_2\bullet6H_2O$ and $(NH_3)_6Mo_7O_{27}\bullet4H_2O$). The solution was left to stir overnight at room temperature. To this solution, 10 mL of 70 % nitric acid was added and left to stir for 2 h at ambient temperature. The solvent was then removed at 120 °C followed by calcination at 300 °C to obtain the dried perovskite material which is crushed to form a powder. These perovskites were then characterized fully with different techniques.

2.2.1. Nitrogen-sorption (BET) measurement
The surface of the prepared perovskite materials was assessed using the Micrometrics ASAP 2460 surface and porosity analyser. Approximately, 0.30 g of the perovskite samples were degassed at100 °C overnight to remove any adsorbed species from the surface of the perovskite catalysts. The samples were left to cool for a short while prior to analysis which was conducted using nitrogen probe gas at −196 °C. From this analysis technique, the pore size, pore volume and surface area of the perovskite catalysts were obtained.

2.2.2. Powder X-ray diffraction (P-XRD)
The crystalline structure of the perovskite catalysts was determine using P-XRD. The fine powder samples were loaded onto the alumina sample holders and irradiated in the Rigaku MiniFlex-600 powder X-ray diffractometer. The diffractometer had a copper radiation source ($CuK\alpha_1$) which had a wavelength of 0.15060 nm. The diffraction pattern of the perovskite was compared to those found in the Match! 2 database to confirm the identity of the perovskite and to gather the crystalline phases.

2.2.3. Scanning electron microscopy (SEM)
The surface morphology of the perovskite catalysts was evaluated using the Tescan Vega3LMH scanning electron microscope. To the sample holder, a double-sided black carbon tape was placed on it and the perovskite samples were mounted onto it. These catalysts were then carbon coated using the Agar Turbo Carbon Coater. These samples were then loaded on the scanning electron microscope.

2.2.4. Inductively coupled plasma – optical emission spectroscopy (ICP-OES)
The determination of the metal composition of the perovskite was assessed using the technique, ICP-OES. The samples were initially digested in aqua regia, 150 mg of each sample. Digestion was carried out at 35 °C for an hour. The digested solutions were later diluted $100\times$ to prepare the sample solution. The standards solutions of Mo, Sr and Ni were prepared at concentrations 100 ppm, 10 ppm and 0.1 ppm. Analysis of the sample to get the percentage composition of the metals in the perovskite was done using the SPECTO

ARCOS smart analyser.

2.2.5. Thermal gravimetric analysis (TGA)

The stability of the perovskites was assessed using the technique, TGA. Approximately 10 mg of the sample was screened for stability at temperatures ranging from 25 to 800 °C with a ramping temperature rate of 10 °C/min in air. This was done using the instrument, PerkinElmer STA 600.

2.2.6. X-ray photoemission spectroscopy (XPS)

The metal oxidation states, and oxygen vacancies were evaluated with the technique, XPS. The samples were first mounted on carbon tapes. Their analysis was carried out in ambient temperatures on the Thermo ESCAlab 250Xi instrument fitted with a monochromatic Al kα (1486.9 eV). The analysis chamber was at a pressure $<10^{-8}$ mbar. The low-energy electron flood gun was set to 20 eV and it was used to charge the surface of the material. The survey pass energy was 100 eV. An X-ray spot size of 900 μm and X-ray power of 300 W. The XPS spectra of the prepared perovskite samples were normalised by background and/or height of the most intense peak to enhance the comparison.

2.3. Catalytic studies: aldol condensation of BAL and DEK

The aldol condensation of benzaldehyde (BAL) and diethyl ketone (DEK) was carried out in a carousel tube. To optimize the condition for this reaction 10 mmol of BAL and 20 mmol of DEK at temperatures between 80 °C and 120 °C in varying perovskite $SrMo_{1-x}Ni_xO_{3-\delta}$ catalysts ($0 \leq x \leq 1$). Difference solvents (dioxane, dimethylformamide, tetrahydrofuran and without a solvent) were also screened for this reaction. The time of the reaction was screen between 5 and 25 h. In every reaction 1 mL of an internal standard, octane or *n*-decane, was used. The progression of the reaction was quantitively and qualitatively monitored using the Shimadzu 2010 Plus GC-FID and GC-MS.

3. Results and discussion

3.1. Synthesis and characterization of multicationic SrMo1-xNixO3-δ inorganic perovskites

3.1.1. Nitrogen-sorption measurements (BET)

Pore size, pore volume and the surface area of the synthesized perovskites were determined by nitrogen-sorption BET analysis. These properties were analysed through the assessment of the isotherms and the pore size distribution curves, as summarised in Fig. 1S. The isotherms in Fig. 1S (a) show that the perovskites have a type IV isotherm with an H2 hysteresis loop, with the exception of $SrMo_{0/3}Ni_{0/7}O_{3-\delta}$ perovskite's isotherm follows a type II isotherm which is indicative of a non-porous material. The nature of the isotherm of the other perovskites compares to those that have been previously reported mesoporous perovskites [36,37]. Fig. 1S (b) shows a zoomed version of the adsorption isotherms in order to rule out the that the material is non-porous. To verify the mesoporosity of the material a cumulative pore size plot, depicted in Fig. 1S (c), showed that the pore size range is within the mesoporous range. The differential pore size distribution plot, illustrated in Fig. 1S (d), which quantifies the amount of micropores, mesopores, and micropores within the perovskite material. The perovskite $SrNiO_3$, has an intense broad peak in the mesoporous range, which affirms that it is a mesoporous material. The other perovskites, $SrMo_{0.7}Ni_{0.3}O_{3-\delta}$ and $SrMo_{0.5}Ni_{0.5}O_{3-\delta}$ have a combination of mesopores and micropores, which is shown by the narrow peak (<2 nm) and a broad peak (>2 nm), however, the area of the peak that is in the mesoporous range is larger than that of the micropores, which makes the overall material mesoporous. As seen in Fig. 1S (a) the perovskites, $SrMo_{0.3}Ni_{0.7}O_{3-\delta}$, was found to be non-porous, and this is still being seen in Fig. 1S (c), indicated by the flat line. The pore sizes of the
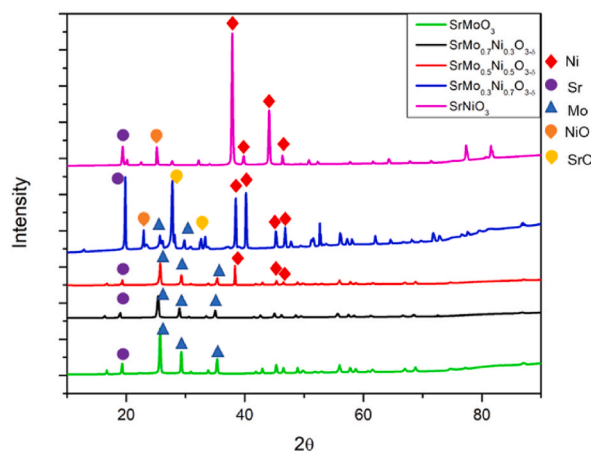
Fig. 1. Wide angle PXRD diffractograms of the synthesized $SrMo_{1-x}Ni_xO_{3-\delta}$ perovskites.

materials are summarised in Table 1 determined at half-length of the pore size distribution curve in Fig. 1S (c). The specific surface area of the perovskite in Table 1 were small as a consequence of the method used and the multiple cations involved [38,39]. Moreover, there is not linear improvement in surface area with respect to the metal cation variations (quantity). As such, $SrMo_{0.5}Ni_{0.5}O_{3-\delta}$ and $SrMo_{0.7}Ni_{0.3}O_{3-\delta}$ inorganic perovskites had the largest and smallest S_{BET}, respectively. It is crucial to note that partial substitution cannot be used as an empirical approach to improve the surface area of the perovskite.

The Grahamschidt equation was used to determine the tolerance factors of the materials. Equations (1) and (2) were used to calculate the tolerance factors of simple ABO_3 perovskites and complex 0.5:0.5 multicationic inorganic perovskites. This calculated is used to determine the stability of the perovskite and the chances of the formation of the perovskite structure. The equation makes use of the ionic radii of the metal cation and the anion and from that the chances of forming that perovskite. These values are summarised in Table 1, and all the perovskites had a tolerance factor of 1.06 which is within the acceptable range for perovskite. Moreover, this value certifies that the perovskites are cubic with extremely minor distortions. Literature also reported $SrMoO_3$ and $SrNiO_3$ to have tolerance factors of 0.986 [43,44] and 1.08 [45], respectively.

$$t = \frac{(r_A + r_o)}{\sqrt{2}(r_B + r_O)} \tag{1}$$

$$t = \frac{(r_A + r_O)}{\sqrt{2\left[\left(\frac{r_B + r_{B'}}{2}\right) + r_O\right]}} \tag{2}$$

3.1.2. Powder X-ray diffraction (PXRD)

The crystallinity of the material was discerned by manner of X-Ray diffraction. The wide-angle diffraction patterns of the prepared inorganic perovskite materials are illustrated in Fig. 1. $SrNiO_3$ and $SrMoO_3$ have peaks which were ascribed to the Ni and Mo in the material. Peaks at 25° and 30° were ascribed to Mo, as they were only observed in the $SrMoO_3$ perovskite diffractogram. Similarly, peaks at 38° was assigned to the Ni in the material as it is only observed for the $SrNiO_3$. The diffraction pattern for the perovskites, $SrNiO_3$ (JCDPS: 75–0197) [42,45] and $SrMoO_3$ (JCDPS: 24–1224) [46], match those that have been previously reported. Therefore, this information can be extrapolated to fit the other multicationic inorganic perovskites. There is a decrease in peak intensity as the as the quantity of the metal cation decreases. For example, $SrMo_{0.3}Ni_{0.7}O_{3-\delta}$ perovskite has a peak for Mo that is very small peak that it is undetectable with this instrument used. However, the peak starts to increase and it prominent until $SrMo_{0.7}Ni_{0.3}O_{3-\delta}$ perovskite, in the multicationic perovskites. The same was also observed for the Ni peaks in the diffractograms of the different multicationic inorganic perovskites.

3.1.3. Transmission electron microscopy (TEM) and scanning electron microscopy (SEM)

The internal and surface morphology of the inorganic perovskites was investigated using TEM and SEM. The dark field TEM images in Fig. 2S (a-e) show no presence of nanoparticles and/or heterostructures. This confirms that the perovskite is one uniform material with no other existing materials. The surface of the synthesized multicationic inorganic perovskites were found to be unusual for perovskites. They displaced irregular rod-like particles with foam-like agglomerations as shown in Fig. 2S (f-j). However, $SrMoO_4$ is reported to have octahedron-like particles, which is a surface that is also unusual for perovskites [47]. This justifies that the prepared perovskites can have been rod-like. The agglomeration observed for the synthesized perovskites is typical of ceramics like $Sm_{0.8}Sr_{0.2}Fe_{1-x}Co_xO_{3-\delta}$ [48].

3.1.4. Inductively coupled plasma – optical emission spectroscopy (ICP-OES)

To quantify and verify the exact quantities of the metal cations in the inorganic perovskite materials, ICP-OES was used to conduct this analysis. A synopsis of this information is shown in Table 1S, from which it can be seen that the amount of Sr is constant throughout all the prepared perovskites. There is an absence of Ni in the $SrMoO_3$ perovskite, which is expected, and there is a negligibly small amount of Mo in the $SrNiO_3$ perovskite which is due to the sample preparation prior to the ICP-OES analysis. The metal ratio between Mo and Ni was calculated and compared as shown in Table 1S, under the column with experimental and expected. The ratio obtained is close to the expected, therefore, it can be deduced that the synthesis was successful.

Table 1

Summary of the nitrogen-sorption measurements of the prepared perovskites and comparison with literature.

Entry	Perovskite	S_{BET} (m^2/g)	Pore size (nm)	Pore volume (cm^3/g)	Tolerance factor	Reference
1	$SrMoO_3$				1.06	This work
2	$SrMoO_4$	1.6	–	–		[40]
3	$SrMoO_3$	7.0				[40]
4	$SrMo_{0.7}Ni_{0.3}O_{3-\delta}$	5.5	6.5	0.02		This work
5	$SrMo_{0.5}Ni_{0.5}O_{3-\delta}$	1.9	7.6	0.02	1.06	
6	$SrMo_{0.3}Ni_{0.7}O_{3-\delta}$	4.5	7.3	0.01		
7	$SrNiO_3$	4.9	9.3	0.03	1.06	
8	$SrNiO_3$	6.2	–	–		[41]
9	$SrNiO_3$	12.2	9.3	0.03		[42]
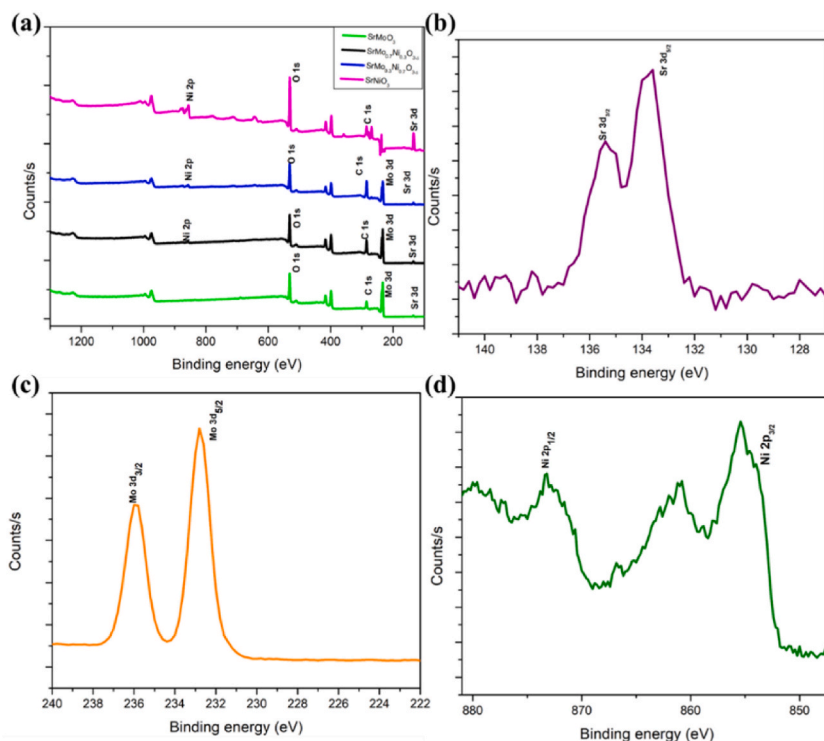
Fig. 2. The XPS survey spectra for the prepared perovskites (a) and deconvoluted peaks of the metals of interest (b–d).

3.1.5. X-ray photoemission spectroscopy (XPS)

The composition alone does not suffice as proof to for successful synthesis of the multicationic perovskites. The XPS survey spectra, illustrated in Fig. 2 (a), shows that the prepared perovskites are comprised of all the desired metals. It is worth noting that the survey spectra of the $SrMoO_3$ perovskite is similar to those found in literature [49,50]. The isolated metal XPS peaks are shown in Fig. 2 (c-d). The Sr 3d spectra in Fig. 2 (b) had a doublet peak at 135.4 eV and 133.6 eV binding energies for Sr $3d_{3/2}$ and Sr $3d_{5/2}$ electrons, respectively. Both peaks are for Sr in its oxidation state 2+. These is in line with $SrMoO_3$ perovskite that was previously reported [49, 51]. This was the same throughout the rest of the other perovskite materials.

The Ni peaks depicted in Fig. 2 (c) is a doublet peak for Ni $2p_{2/3}$ and Ni $2p_{1/2}$ electrons at binding energies 855.5 eV and 873.3 eV, respectively. This corresponds to Ni in its oxidation state of 2+ [45]. There are satellite peaks at binding energies above 860 eV were expected and are observed [52,53].

Fig. 2 (d) shows the doublet peak for Mo $3d_{3/2}$ and $3d_{5/2}$ at binding energies 235.9 eV and 232.8 eV, respectively. At these binding energies Mo exists in two oxidation states, +4 and + 6. This leads to the possibility of forming the scheelite, $SrMoO_4$, and the perovskite, $SrMoO_3$. The prevalence of Mo^{6+} will result in a largess of $SrMoO_4$ forming, and when Mo^{4+} ions are dominant, then more $SrMoO_3$ will be dominant. This assessment was done by comparing the ratio of the areas of the two peaks. This is summarised in
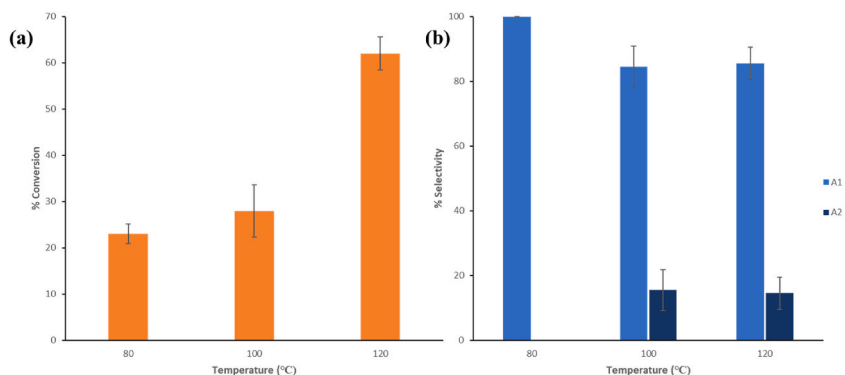
Fig. 3. Temperature effects on the (a) conversion and (b) product selectivity of 10 mmol of BAL to yield aldol condensation products. Reaction condition: 10 mmol BAL and 20 mmol in 4 mL of 1,4-dioxane with 100 mg $SrMoO_3$ perovskite catalyst for 20 h.

Table 3S, and from this it was found that since over 70 % of the peak is attributes to the prevalence of SrMoO₃. This observation also emphasizes the nature of the distortions that take place as a consequence of multiple cations being present in the perovskite lattice structure.

These distortions are a consequence of or induce oxygen defects. To evaluate the nature of the oxygen defect, the O 1s peak was deconvoluted as shown in Fig. 3S. The deconvoluted peaks represent the metal oxide, surface adsorbed oxygen and oxygen vacancies, which are the defects to be analysed. The area of the oxygen vacancies deconvoluted peaks, abridged in Table 2, were compared. It was found that SrMoO₃, SrMo₀.₅Ni₀.₅O₃₋δ and SrNiO₃ had the highest amount of oxygen vacant sites, and the former two, had a similar Mo^{4+}/Mo^{6+}ratio, which shows the severity of the distortions.

3.1.6. Thermal gravimetric analysis (TGA)

Beyond the tolerance factor, the stability of the perovskite was analysed by manner of TGA. Although the degradation temperature used in below temperature in which the reactions will be conducted. Fig. 4S illustrates the TGA thermograms of the prepared perovskites and they all had a similar degradation trend. There is dehydration of weakly and strongly bound water molecules and organic matter from the synthesis. The perovskites SrMoO₃, SrMo₀.₅Ni₀.₅O₃₋δ and SrNiO₃ were found to possess the same decomposition profiles. The rest of the perovskites showed dramatic decomposition profiles which could be ascribed to the decomposition of the surfactant [54] and MoO₃ decomposition [55,56] and/or that of NiO [57,58].

3.2. Solvent-free aldol condensation benzaldehyde with diethyl ketone with inorganic multicationic SrMo1-xNixO3-δ perovskite as catalyst

The synthesized multicationic perovskites were then used as catalysts for the transformation of bio-derived molecules in an aldol condensation reaction. This reaction extends the chain length and has wide applications in the pharmaceutical industry and a potential precursor step to synthesizing long chain hydrocarbons in the petrochemical industry. The reaction of benzaldehyde (BAL) with diethyl ketone (DEK) was used as a model reaction to demonstrate the capabilities of the SrMo₁₋ₓNiₓO₃₋δ multicationic perovskites.

3.2.1. Influence of temperature

. In heterogeneous catalysis, aldol condensation is conducted at temperatures as high as 350 °C with zeolite H-ZSM-35 [26] and as low as 50 °C with La^{3+} organic zeolite with other additives [28] with good yield after 4 and 85 h, respectively. Herein, BAL and DEK using dioxane as a solvent was screened from 80 °C to 120 °C in the presence of SrMoO₃ perovskite catalyst shown in Fig. 3. The possible products that can emanate from this reaction are shown in Scheme 1. These products are predicted based on the mechanism of the aldol condensation reaction which requires the abstraction of the α-proton. As such, there is a chance of self-aldol condensation, cross aldol condensation and the cross-aldol condensation occurring twice.

The temperature of the reaction was varied while the amount of catalyst and solvent were held constant, and the results obtained are reported in Fig. 3. An increase in temperature has a positive influence on many catalytic systems. In aldol condensation, an increase in temperature increases the rate at which the substrate is being transformed [35,59,60]. A heterogeneous Mg/Al metal oxide catalyst was evaluated for an aldol condensation with furfural and acetone by Parejas and co-worker, and they observed that an increase in temperature increased the amount of furfural converted [61]. The effects of temperature on the aldol condensation of benzaldehyde (BAL) and diethyl ketone (DEK) are summarised in Fig. 3a. The activity of the SrMoO₃ catalyst in facilitating the aldol condensation between these two carbonyl-containing compounds was as low as 23 % BAL conversion at 80 °C which then increased to 63 % when temperature was raised to 120 °C. This increase in temperature is consistent with previously reported results.

The nature of an aldol condensation reaction to transform carbonyl-containing compounds to α,β-unsaturated ketones is likely to result in many side products. In this reaction, the carbonyl containing substrates used were benzaldehyde (BAL) and diethyl ketone (DEK). From these, DEK undergoes self-aldol condensation to give products **A5** as shown in Scheme 1. The product **A1** can undergo a second round of aldol condensation with BAL to give product **A4**. This is because of the α-hydrogen present in **A1**. However, product **A1** can form an aldol product with DEK instead of BAL to give aldol product **A3**. The selectivity of the reaction towards a certain aldol product will, therefore, be governed by the environment in which the reaction is taking place. Temperature is one of the reaction parameters which has an influence on the selectivity of the reaction. The effect of temperature on the selectivity of the aldol condensation with SrMoO₃ perovskite in dioxane was conducted (shown in Fig. 3 (b)). From this there is a 100 % selectivity towards aldol product **A1** at 80 °C. When temperature is increase to 100 and 120 °C, the selectivity towards **A1** is slightly reduced with the formation of a new aldol product **A2**. The decrease in selectivity with increasing temperature was also observed by Liang and co-

Table 2

The binding energies of the core level O1s metal oxide and oxygen vacancies peaks for the synthesized SrMo₁₋ₓNiₓO₃₋δ perovskite and the peak area of the oxygen vacancy peak.

Entry	Perovskite	Binding energy (eV)		Area of oxygen vacancy
		Metal oxide	Oxygen vacancy	
1	SrMoO₃	530.632	531.433	14145.792
2	SrMo₀.₇Ni₀.₃O₃₋δ	530.620	531.508	13746.724
3	SrMo₀.₅Ni₀.₅O₃₋δ	530.593	531.296	14435.634
4	SrMo₀.₃Ni₀.₇O₃₋δ	530.338	531.232	13878.989
5	SrNiO₃[a]	530.896	531.976	13983.828
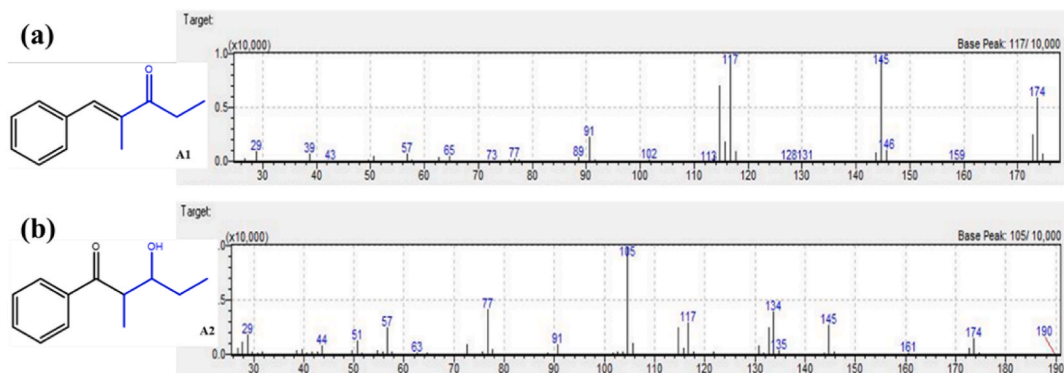
Fig. 4. Fragmentation patterns of aldol condensation products (a) **A1** and (b) **A2**. Reaction condition: 10 mmol BAL and 20 mmol in 4 mL of 1,4-dioxane with 100 mg SrMoO$_3$ perovskite catalyst for 20 h.
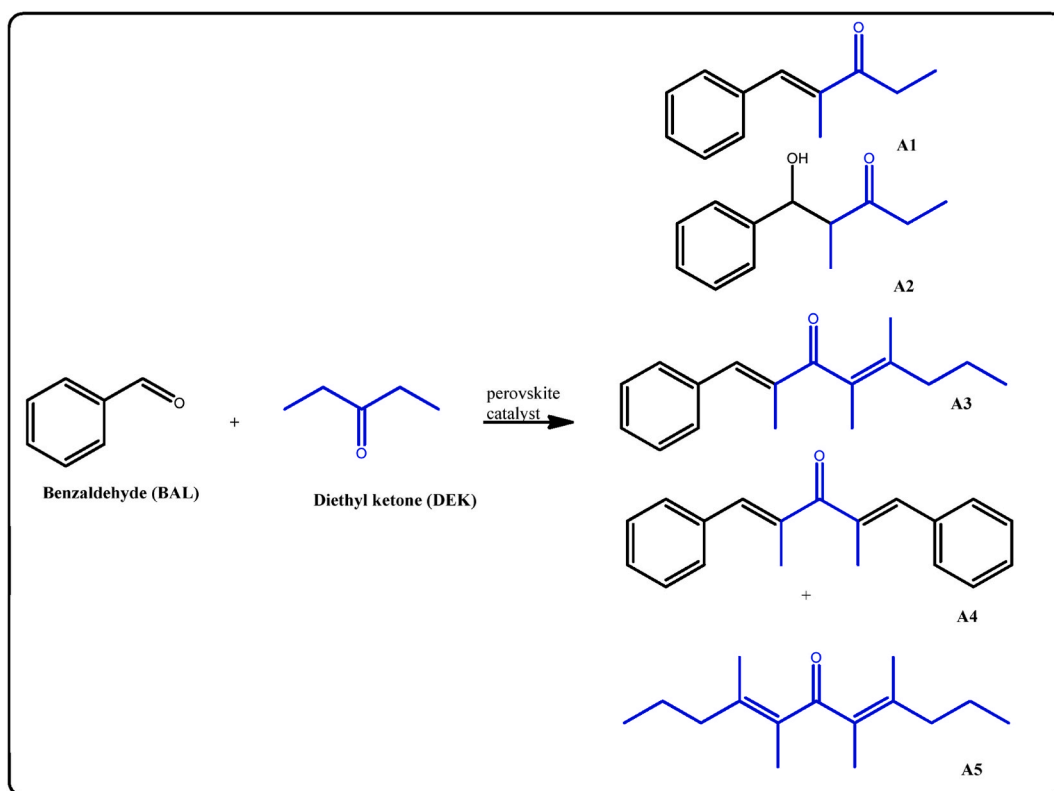
Scheme 1. Illustration of the potential products of the aldol condensation reaction of benzaldehyde (BAL) and diethyl ketone (DEK) with solid perovskite catalyst.

worker on their work on self-aldol condensation of cyclopentanone over metal oxide catalysts [62]. The catalyst reported by Lian and co-worker, MgO–ZrO$_2$, favours the self-aldol condensation of cyclopentanone whereas, the perovskite SrMoO$_3$ used herein favoured the cross-aldol condensation between DEK and BAL.

There were no differences observed in the **A1** and **A2** selectivity at 100 °C and 120 °C. Both **A1** and **A2** are aldol condensation products, which shows that SrMoO$_3$ can facilitate this reaction. It was then decided that 120 °C is the optimum temperature due to the high percentage conversion of BAL at this temperature.

The fragmentation patterns of the products were deciphered to confirm the structures of the products obtained. The GC-MS was used for isolating the aldol products and give their fragmentation patterns. The fragmentation patterns of **A1** and **A2** aldol products are shown in Fig. 4. The fragment peak at 174 m/z matches the molecular weight of aldol product **A1**. Moreover, the fragment peaks at 117 and 57 m/z (shown in Fig. 4 (a)) are those when the bond between the carbonyl carbon and the α-carbon of the alkene bond is spliced.

The fragment containing the methyl group (117 m/z) can further cleave off the methyl to give the fragment 102 m/z, which is shown in Fig. 4 (a). When the bond between the carbonyl carbon and that of –CH$_2$CH$_3$ is cut, the fragments that arise from this are 145 and 29 m/z which are seen in the fragmentation patterns of **A1** in Fig. 4 (a). The second product, **A2**, was also analysed using GC-MS to identify the product. The fragmentation patterns of **A2** are shown in Fig. 4 (b), and from this there is the presence of the 77 m/z fragment which indicates that the product may contain a benzene ring. Further analysis provided evidence that cleavage between the hydroxyl group and the methyl substituent, gives the 107 m/z fragment, which gives base peak 105 m/z when H is cleaved off. Fragmentation between the carbonyl and the methyl branch, gives fragments 135 m/z and 37 m/z which can also be seen in this fragmentation patterns. Aldol product **A2** is the intermediate product for **A1**.

3.2.2. Catalyst variation with respect to temperature

Different catalysts will perform differently at different temperatures. This is because temperature influences the orientation of the substrate on the surface of the heterogeneous catalyst and the residence time of the substrate on the catalyst surface. It, therefore, influences the overall conversion of the substrate to produce a product. The multicationic perovskites SrMo$_{1-x}$Ni$_x$O$_{3-\delta}$ ($0 \leq x \leq 1$), were screened as catalysts for the aldol condensation at varying temperatures. As shown in Fig. 5, there was no conversion observed in the absence of a catalyst. This is due to the fact that the first step of this reaction requires the formation of an enol which depends on the abstraction of the α-hydrogen by the base. This was also observed by Chen and co-workers in their aldol condensation in dioxane [63]. In the presence of the perovskite catalysts, conversion of the substrates was observed (see Fig. 5 (a)). There is a clear increase in the activity of all the used perovskite catalysts with an increase in temperature. This is an indication that the rate of this aldol condensation is dependent on temperature [61]. In this aldol condensation, the perovskites, SrMoO$_3$ and SrNiO$_3$, were found to be effective catalysts; however, their activities were enhanced when Ni and Mo, respectively, were incorporated into the perovskite structures. Both Ni and Mo have been used in variants of aldol condensation reaction and were found to be fairly active above 200 °C [15,64–66]. In this work, multicationic perovskites catalysts, SrMo$_{0.3}$Ni$_{0.7}$O$_{3-\delta}$ and SrMo$_{0.7}$Ni$_{0.3}$O$_{3-\delta}$ were used at 80 °C. Their activities were lower than that of SrMoO$_3$ and SrNiO$_3$. When the reaction temperature was raised to 100 °C and 120 °C, the SrMo$_{0.3}$Ni$_{0.7}$O$_{3-\delta}$ perovskite had a better activity, however, the activity of the SrMo$_{0.3}$Ni$_{0.7}$O$_{3-\delta}$ only started to surpass the activity of SrNiO$_3$ at 120 °C. When the ratio between the two metals is 50:50 in the crystal lattice of the perovskite (SrMo$_{0.5}$Ni$_{0.5}$O$_{3-\delta}$), the activity consistently surpassed that of the other perovskite catalysts (shown in Fig. 5 (a)). This perovskite had the lowest surface areas and highest amount oxygen vacancies of these perovskites, which were discussed in Tables 1 and 2, respectively. The perovskites, SrMo$_{0.3}$Ni$_{0.7}$O$_{3-\delta}$ (4.5 m^2/g), SrMo$_{0.7}$Ni$_{0.3}$O$_{3-\delta}$ (5.5 m^2/g), and SrNiO$_3$ (4.9 m^2/g) had the largest surface areas of the bunch, however they were also the perovskites that gave the lowest catalytic conversions, whereas the perovskite with lowest surface area SrMo$_{0.5}$Ni$_{0.5}$O$_{3-\delta}$ gave the highest conversions. In catalysis, it is expected that the material with a high surface area to also give the highest catalytic conversion [67]. However, some literature also shows that materials with the highest surface areas gave low catalytic conversion [36,67,68].

The selectivity trends of the reaction with varied temperature and catalyst are shown in Fig. 5 (b). Herein, it was observed that the temperature had a major influence on the formation of **A1**. The selectivity of **A1** with respect to the catalyst was found to be the same throughout. At 80 °C, all catalysts gave 100 % selectivity towards **A1**, and we postulate that the temperature is low enough to facilitate the transition and the reaction time also allows the formation of **A1**. The decline in selectivity, as seen in Fig. 3, is due to the temperature increase. The SrNiO$_3$ perovskite gave highest selectivity when the temperature was increased, which is a trait that speaks to the preferential binding of the substrate to this catalyst. Although this is the case, the selectivity of all 5 perovskite catalysts was found to be above 80 % towards **A1**, which is a remarkable observation for cross-aldol condensation.

The oxygen vacancies did not show any trend with respect to the catalytic conversions of the substrates. This is deduced from the perovskite catalysts with the highest oxygen vacancies, SrMoO$_3$ and SrMo 0.5Ni0.5O$_{3-\delta}$, produced both the lowest and conversions.
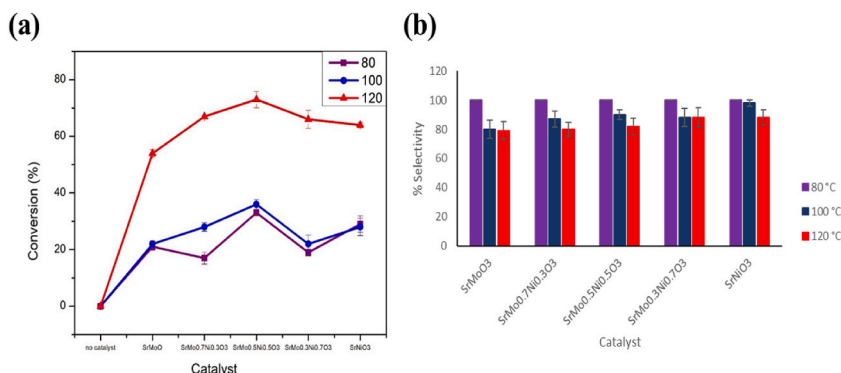
Fig. 5. (a) Performance of several SrMo$_{1-x}$Ni$_x$O$_{3-\delta}$ perovskite catalysts in aldol condensation reaction between benzaldehyde (BAL) and diethyl ketone (DEK) and (b) selectivity towards **A1** at different temperatures. Reaction condition: 10 mmol BAL, 20 mmol DEK, 1 mL n-decane internal standard, 4 mL dioxane and 100 mg perovskite catalyst for 20 h.

3.2.3. Thermodynamic study

The spontaneity of the reaction is gauged by determining the thermodynamic parameters of the reaction. The change in enthalpy (ΔH) and change in entropy (ΔS) of aldol reaction between BAL and DEK was calculated using the linearized Arrhenius equation (3) [69]. This plot produced from this equation shown in Fig. 5S, was used to calculate the thermodynamic parameters and Gibb's free energy was extrapolated from the utilization of the ΔH and ΔS at optimal temperature using equation (4).

$$\ln(\%conversion) = \frac{-\Delta H}{R} \times \frac{1}{T} + \frac{\Delta S}{R} \qquad\qquad 3$$

$$\Delta G = \Delta H - T\Delta S \qquad\qquad 4$$

This aldol condensation reaction was found to have a negative ΔH which indicates that the reaction is exothermic. The exothermic nature of an aldol condensation reaction is also observed in literature (Table 3S entries 6–8). Contrary to literature, the magnitude of the energy released (ΔH) was found to be higher than those reported which mean that the reaction becomes highly exothermic in the presence of the multicationic perovskites. The change in entropy (ΔS) for this reaction was found to be negative as well. A negative ΔS indicates that there is a decrease in the overall disorder of the reaction, which is translated to fewer collisions between the reactant molecules. Fewer collisions between the substrate molecules, results in far fewer products that could emanate from this reaction. This, therefore, explains the two products which were obtained at these conditions. Moreover, the magnitude of ΔS is so small in comparison to ΔH, so this will not affect the overall spontaneity of the reaction. The Gibb's free energy of this aldol condensation reaction was found to be negative, across all the multicationic inorganic perovskites used, and this value speaks to the spontaneity of the reaction, and this is also seen in literature.

3.2.4. Solvent screening

Solvent has an influence on the chemoselectivity of the product and thus has an influence on the thermodynamic and kinetic products that can be generated during the course of the reaction. The effect of different solvent such as dimethylformamide (DMF), dioxane, tetrahydrofuran (THF), and no solvent on the overall conversion of the substrate were studied and the results are shown in Fig. 6. According to Capello and co-worker, the order in which the solvents are green is as follows: no solvent > dioxane > DMF > THF [70]. The reaction was conducted at 120 °C using the multicationic perovskite SrMo$_{0.5}$Ni$_{0.5}$O$_{3-\delta}$ as the catalyst. The solvents had a huge impact on the overall reaction.

Both THF and dioxane gave the lowest conversions compared to DMF (see Fig. 6 (a)). Although DMF has been reported as a good solvent for cross aldol condensation, reactions in DMF using organocatalyst was found to give poor conversions in comparison to THF [71–73]. Even so, a study conducted by Chen and co-workers found that an aldol condensation of BAL and a cyclic ketone was better in DMF than in THF [63]. The latter corroborates the results obtained in this aldol condensation. According to Chen and co-worker, DMF behaves as a weak base which improves the efficacy of the perovskite catalyst in this reaction [63]. The best solvent to use for any reaction, is no solvent at all. This is because it is the greenest solvent to use. From Fig. 6 (a) it is observed that this reaction in the absence of the solvent was found to be better than when THF and dioxane were used, however, not better than DMF. The order of activity for this aldol condensation reaction in these organic solvents is DMF > no solvent > dioxane > THF. The reason for this behaviour is not clear, however, we suspect that THF and dioxane competitively bind to the active site of the perovskite catalyst, thus inhibiting the aldol reaction. Alternately, the two solvents bind intently on the surface of the perovskite which interferes with the interaction of BAL and DEK. The basicity of DMF does help improve the activity of the perovskite catalyst. In the absence of DMF (no solvent), as shown in Fig. 6 (a), there was a drop in conversion of about 4 %. Given the circumstance, this was not a significant decline. Furthermore, having no solvent is a greener approach, therefore no solvent was considered as the best course of action.

The above covers the activity of the catalysts in different solvent environment, but product selectivity has not been explained. Fig. 6 (b) shows the influence of these solvents on the type of product that forms. The type of solvent has an influence on the product which forms. With the exception of dimethylformamide (DMF) which gave three products, only two products were observed when the other organic solvents were used in this aldol condensation reaction, as shown in Fig. 6 (b). The aldol product **A1** was the most prevalent and
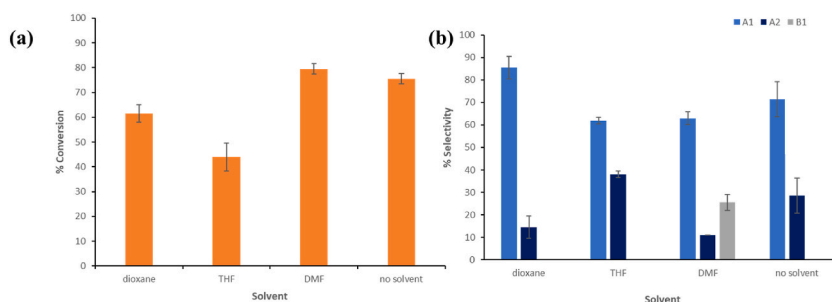
Fig. 6. Influence of different organic solvents on the (a) conversions of substrates and (b) product selectivity for aldol condensation reaction. Reaction condition: 10 mmol BAL, 20 mmol DEK, 1 mL n-decane internal standard, 4 mL of organic solvent and 100 mg SrMo$_{0.5}$Ni$_{0.5}$O$_{3-\delta}$ perovskite catalyst at 120 °C for 20 h.

therefore the major aldol product in this aldol condensation reaction. It is worth noting that this was the target aldol product. In DMF, a third product, **B1** (shown in scheme 1S), was obtained. This product is suspected to come from the decarbonylation of DMF to produce dimethylamine which then reacts with BAL to give dimethylbenzamide, following the reaction scheme 1S.

Samudrala and co-workers reported the use of DMF as a reactant at 80 °C in the presence of an oxidant to yield benzamide, whereas Liu ad co-workers reported the formation of thioamides from aldehydes and DMF at 120 °C in the presence of a base [63,74–76]. The decarboxylation of DMF to produce dimethylamine is an *in-situ* reaction which occurs at a 120 °C in the presence of a base [76]. In this reaction, no additive was introduced into the system even though benzamide (**B1**) was produced. The dimethyl benzamide was confirmed using fragmentation patterns obtained from GC-MS. The fragmentation pattern of **B1** shown in Fig. 6S has a base peak of 121 m/z which is obtained from the removal of the two methyl substituents. An additional cleavage of the carbonyl oxygen, gives fragment of 105 m/z, seen in the fragmentation pattern in Fig. 6S. To confirm that this reaction occurred between BAL and DMF instead of DEK, is due to the 77 m/z fragment which emanates from the cleavage between the phenyl ring and amide function group. The 77 m/z fragmentation piece is the benzene ring.

3.2.5. Time study

The time at which the reaction reaches completion is another crucial step to account for to determine the rate of the reaction. The aldol condensation between BAL and DEK was assessed at different times to generate the time vs. percentage conversion and percentage selectivity plots in Fig. 7S. From the plots, it is clear that there is an increase in percentage conversion as time increases, however, it begins to plateau between 20 and 25 h. Interestingly, a similar trend was also observed for selectivity. Selectivity towards the desired cross aldol product **A1** seemed to increase with time. This suggests that the other product **A2** is an intermediate product which lead to the formation of the aldol product **A1**. The selectivity also seems to depend on how much of BAL has been converted. This is observed with the presence of both **A1** and **A2**, and even **B1**, in the reaction mixture at the end of the reaction. All the products obtained from this aldol condensation reaction had BAL in their resulting structure, therefore suggesting that the reaction is ruled by the conversion of BAL.

3.2.6. Reaction mechanism

We postulate that the reaction proceeds as that proposed by Cosimo and co-worker, where the carbonyl moiety of DEK adsorbs to the metal cation (M^{n+}) site and the alpha hydrogen adsorbs to oxygen anion [77]. This adsorption leads to the detachment of this alpha hydrogen and the formation of the carbanion intermediate, as shown Fig. 7. This carbanion intermediate then attacks the carbonyl functional group of BAL. The ion that forms which then abstract the proton on the surface of the catalyst to form product **A2**. Another round of alpha proton abstraction by the catalyst from **A2**, and this proton will be abstracted by the hydroxyl group on **A2**. Lastly, H_2O is released [9], and the electron migrate to form the double bond and product **A1**.

4. Conclusions

This work has demonstrated that the soft-templating method is one that results in successful synthesis of the multicationic inorganic perovskites $SrMo_{1-x}Ni_xO_{3-\delta}$. Albeit this method results in small S_{BET}, the other properties of these perovskite were found of good standard for mesoporous perovskites with an excellent surface which will cater to their application as heterogeneous catalysts. The coordination of the perovskite was confirmed with the use of XPS which proved to be a useful tool, especially for multicationic inorganic perovskites with a novel combination of metals. In this aldol condensation of BAL and DEK, it was found that all five catalysts showed activity towards the cross-aldol condensation product with the temperature and solvent influencing the overall selectivity of the reaction. The mutlicationic perovskite that performed optimally was found to be $SrMo_{0.5}Ni_{0.5}O_{3-\delta}$, which had the highest amount of oxygen vacances. Although this is true, there was no linear trend in activity with respect to the oxygen vacancies. It is recommended that DMF be avoided for as a solvent for this reaction as it results in the formation of a complex amide with BAL. The activity of the catalyst was found to be competitively high with DMF and without a solvent, however, there were only two products forming with the latter, making it the preferred approach for this study. The selectivity towards **A1** was found to increase with time, whereas **A2** decreased, which indicates that **A2** is the intermediate product.

Data availability statement

Has data associated with this study been deposited into a publicly available repository? No.
Data will be made available on request.

CRediT authorship contribution statement

Lebohang Kekana: Conceptualization, Data curation, Formal analysis, Investigation, Validation, Writing – original draft, Writing – review & editing. **Ndzondelelo Bingwa:** Conceptualization, Data curation, Formal analysis, Funding acquisition, Investigation, Methodology, Project administration, Supervision, Validation, Writing – original draft, Writing – review & editing.

Declaration of competing interest

The authors declare that they have no known competing financial interests or personal relationships that could have appeared to
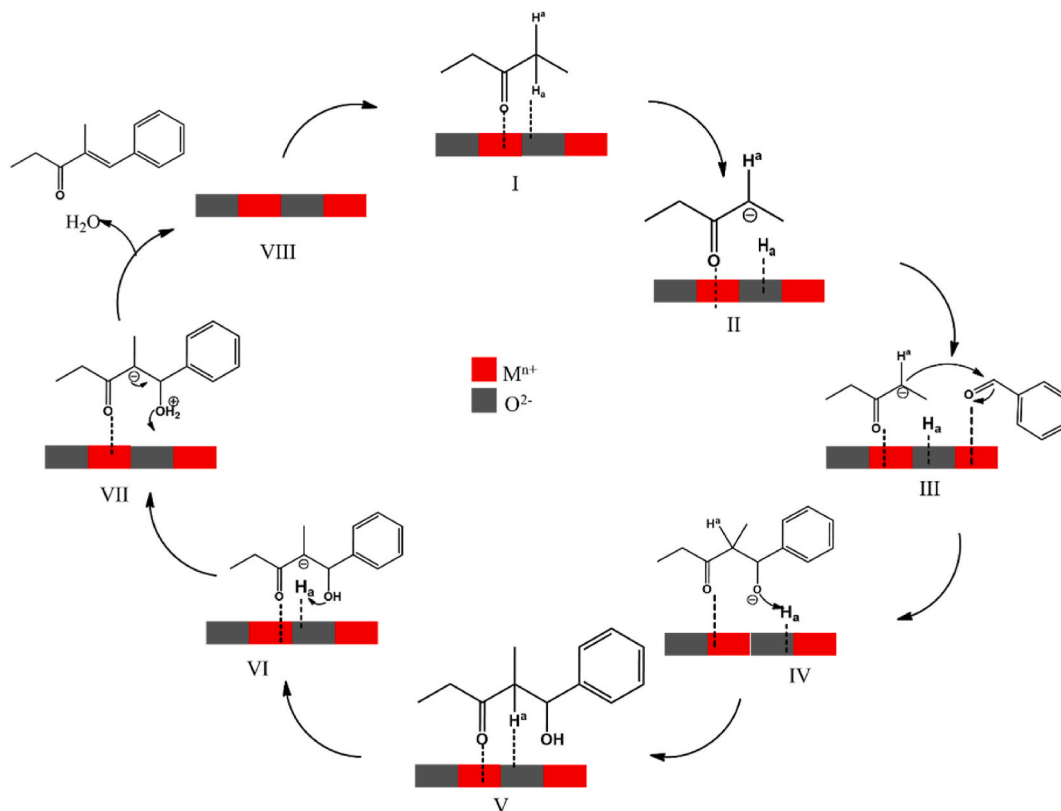
Fig. 7. Proposed reaction mechanism for the aldol condensation between BAL and DEK.

influence the work reported in this paper.

Acknowledgements

Appendix A. Supplementary data

Supplementary data to this article can be found online at https://doi.org/10.1016/j.heliyon.2023.e21038.

References

[1] L.Q. Jiang, J.K. Guo, H.B. Liu, M. Zhu, X. Zhou, P. Wu, C.H. Li, Prediction of lattice constant in cubic perovskites, J. Phys. Chem. Solid. 67 (2006) 1531–1536, https://doi.org/10.1016/j.jpcs.2006.02.004.

[2] Q. Sun, W.J. Yin, Thermodynamic stability trend of cubic perovskites, J. Am. Chem. Soc. 139 (2017) 14905–14908, https://doi.org/10.1021/jacs.7b09379.

[3] E. Grabowska, Selected perovskite oxides: characterization, preparation and photocatalytic properties-A review, Appl. Catal., B 186 (2016) 97–126, https://doi.org/10.1016/j.apcatb.2015.12.035.

[4] R.J. Sutton, M.R. Filip, A.A. Haghighirad, N. Sakai, B. Wenger, F. Giustino, H.J. Snaith, Cubic or orthorhombic? Revealing the crystal structure of metastable black-phase CsPbI3 by theory and experiment, ACS Energy Lett. 3 (2018) 1787–1794, https://doi.org/10.1021/acsenergylett.8b00672.

[5] C. Lin, Y. Zhang, J. Liu, X. Li, Y. Li, L. Tang, L. Xiong, Pressure-induced structural change in orthorhombic perovskite GdMnO 3, J. Phys. Condens. Matter 24 (2012), https://doi.org/10.1088/0953-8984/24/11/115402.

[6] Y. Liu, W. Wang, X. Xu, J.P. Marcel Veder, Z. Shao, Recent advances in anion-doped metal oxides for catalytic applications, J Mater Chem A Mater 7 (2019) 7280–7300, https://doi.org/10.1039/C8TA09913H.

[7] S. Mandal, S. Mandal, S.K. Ghosh, A. Ghosh, R. Saha, S. Banerjee, B. Saha, Review of the aldol reaction, Synth. Commun. 46 (2016) 1327–1342, https://doi.org/10.1080/00397911.2016.1206938.

[8] S. Mandal, S. Mandal, S.K. Ghosh, P. Sar, A. Ghosh, R. Saha, B. Saha, A review on the advancement of ether synthesis from organic solvent to water, RSC Adv. 6 (2016) 69605–69614, https://doi.org/10.1039/c6ra12914e.

[9] C.L. Perrin, K.L. Chang, The complete mechanism of an aldol condensation, J. Org. Chem. 81 (2016) 5631–5635, https://doi.org/10.1021/acs.joc.6b00959.

[10] R.D. Pace, L. Mcwilliams, R.D. Pace, Perkin Reaction: Rapid and Efficient Process Optimization through a Microwave/Design of Experiments Couple, 2006.

[11] D. Rani, P. Singla, J. Agarwal, 'Chitosan in water' as an eco-friendly and efficient catalytic system for Knoevenagel condensation reaction, Carbohydr. Polym. 202 (2018) 355–364, https://doi.org/10.1016/j.carbpol.2018.09.008.

[12] R. Pandey, D. Singh, N. Thakur, K.K. Raj, Catalytic C-H bond activation and Knoevenagel condensation using pyridine-2,3-dicarboxylate-based metal-organic frameworks, ACS Omega 6 (2021) 13240–13259, https://doi.org/10.1021/acsomega.1c01155.

[13] T. Yuan, X. Ye, P. Zhao, S. Teng, Y. Yi, J. Wang, C. Shan, L. Wojtas, J. Jean, H. Chen, X. Shi, Regioselective crossed aldol reactions under mild conditions via synergistic gold-iron catalysis, Chem 6 (2020) 1420–1431, https://doi.org/10.1016/j.chempr.2020.03.014.

[14] A. Hashmi, Cross-Aldol condensation of isobutyraldehyde and formaldehyde using phase transfer catalyst, J. Saudi Chem. Soc. 20 (2016) S382–S386, https://doi.org/10.1016/j.jscs.2012.12.012.

[15] E. Vrbková, T. Kovárová, E. Vyskočilová, L. Červený, Heterogeneous catalysts in the aldol condensation of heptanal with cyclopentanone, Prog. React. Kinet. Mech. 45 (2019), https://doi.org/10.1177/1468678319825713.

[16] K.N. Tayade, M. Mishra, A study on factors influencing cross and self product selectivity in aldol condensation over propylsulfonic acid functionalized silica, Catal. Sci. Technol. 3 (2013) 1288–1300, https://doi.org/10.1039/c3cy20613k.

[17] V.S.R. Ganga, S.H.R. Abdi, R.I. Kureshy, N.U.H. Khan, H.C. Bajaj, P-Toluene sulfonic acid (PTSA)-MCM-41 as a green, efficient and reusable heterogeneous catalyst for the synthesis of jasminaldehyde under solvent-free condition, J. Mol. Catal. Chem. 420 (2016) 264–271, https://doi.org/10.1016/j.molcata.2016.04.030.

[18] J. Hu, Z. Lu, H. Yin, W. Xue, A. Wang, L. Shen, S. Liu, Aldol condensation of acetic acid with formaldehyde to acrylic acid over SiO2-, SBA-15-, and HZSM-5-supported V-P-O catalysts, J. Ind. Eng. Chem. 40 (2016) 145–151, https://doi.org/10.1016/j.jiec.2016.06.018.

[19] A. Wang, J. Hu, H. Yin, Z. Lu, W. Xue, L. Shen, S. Liu, Aldol condensation of acetic acid with formaldehyde to acrylic acid over Cs(Ce, Nd) VPO/SiO2 catalyst, RSC Adv. 7 (2017) 48475–48485, https://doi.org/10.1039/c7ra09778f.

[20] A. Wang, C. Ye, D. Yu, Y. Ding, H. Yin, Synthesis of acrylic acid through aldol condensation of acetic acid with formaldehyde catalyzed by Bi-,W- and Cs-doped B2O3/SiO2 nanocomposites, J. Chem. Technol. Biotechnol. 97 (2022) 1665–1675, https://doi.org/10.1002/jctb.7032.

[21] S. Ghosh, S.S. Acharyya, Y. Yoshida, T. Kaneko, Y. Iwasawa, T. Sasaki, Nontraditional aldol condensation performance of highly efficient and reusable Cs+Single sites in β-zeolite channels, ACS Appl. Mater. Interfaces 14 (2022) 18464–18475, https://doi.org/10.1021/acsami.2c01312.

[22] Q.N. Tran, O. Gimello, N. Tanchoux, M. Ceretti, S. Albonetti, W. Paulus, B. Bonelli, F. Di Renzo, Transition metal b-site substitutions in laalo3 perovskites reorient bio-ethanol conversion reactions, Catalysts 11 (2021) 1–17, https://doi.org/10.3390/catal11030344.

[23] D. Bharali, R. Devi, P. Bharali, R.C. Deka, Synthesis of high surface area mixed metal oxide from the NiMgAl LDH precursor for nitro-aldol condensation reaction, New J. Chem. 39 (2015) 172–178, https://doi.org/10.1039/c4nj01332h.

[24] P. Mäki-Arvela, N. Shcherban, C. Lozachmeur, K. Eränen, A. Aho, A. Smeds, N. Kumar, J. Peltonen, M. Peurla, V. Russo, K.P. Volcho, D.Y. Murzin, Aldol condensation of cyclopentanone with valeraldehyde over metal oxides, Catal. Lett. 149 (2019) 1383–1395, https://doi.org/10.1007/s10562-019-02701-1.

[25] N. Sudheesh, S.K. Sharma, R.S. Shukla, Chitosan as an eco-friendly solid base catalyst for the solvent-free synthesis of jasminaldehyde, J. Mol. Catal. Chem. 321 (2010) 77–82, https://doi.org/10.1016/j.molcata.2010.02.005.

[26] T. Komatsu, M. Mitsuhashi, T. Yashima, Aldol Condensation Catalyzed by Acidic Zeolites, n.d..

[27] J. Kim, S.H. Jin, K.K. Kang, Y.M. Chung, C.S. Lee, Preparation of chemically uniform and monodisperse microparticles as highly efficient solid acid catalysts for aldol condensation, Chem. Eng. Sci. 175 (2018) 168–174, https://doi.org/10.1016/j.ces.2017.09.052.

[28] T. Dewa, T. Saiki, Y. Aoyama, Enolization and Aldol reactions of ketone with a La3+-immobilized organic solid in water. A microporous enolase mimic [4], J. Am. Chem. Soc. 123 (2001) 502–503, https://doi.org/10.1021/ja001140b.

[29] A. Balog, C. Harris, K. Savin, X.G. Zhang, C. Chou, S.J. Danishefsky, A Novel Aldol Condensation with 2-Methyl-4-Pentanal and its Application to an Improved Total Synthesis Epithilone B, 1998.

[30] D.R. Williams, P.P. Nag, N. Zorn, Strategies for the Synthesis of the Novel Antitumor Agent Peloruside A, n.d..

[31] H. Maurya, Current application of aldol condensation in bioinorganic and medicinal chemistry, Maebaldolreaction 1 (2014) 1–29.

[32] X. Kong, X. jie Wei, L. ping Li, Z. Fang, H. Lei, Production of liquid fuel intermediates from furfural via aldol condensation over La2O2CO3-ZnO-Al2O3 catalyst, Catal. Commun. 149 (2021), https://doi.org/10.1016/j.catcom.2020.106207.

[33] R.S. Malkar, H. Daly, C. Hardacre, G.D. Yadav, Aldol condensation of 5-hydroxymethylfurfural to fuel precursor over novel aluminum exchanged-dtp@zif-8, ACS Sustain. Chem. Eng. 7 (2019) 16215–16224, https://doi.org/10.1021/acssuschemeng.9b02939.

[34] J. Cueto, P. Rapado, L. Faba, E. Díaz, S. Ordóñez, From biomass to diesel additives: hydrogenation of cyclopentanone-furfural aldol condensation adducts, J. Environ. Chem. Eng. 9 (2021), https://doi.org/10.1016/j.jece.2021.105328.

[35] W. Wang, X. Ji, H. Ge, Z. Li, G. Tian, X. Shao, Q. Zhang, Synthesis of C15 and C10 fuel precursors with cyclopentanone and furfural derived from hemicellulose, RSC Adv. 7 (2017) 16901–16907, https://doi.org/10.1039/c7ra02396k.

[36] Y. Nzuzo, A. Adeyinka, E. Carleschi, B.P. Doyle, N. Bingwa, Effect of d: Z 2orbital electron-distribution of La-based inorganic perovskites on surface kinetics of a model reaction, Inorg. Chem. Front. 8 (2021) 3037–3048, https://doi.org/10.1039/d1qi00297j.

[37] A.G. Margellou, I.T. Papadas, D.E. Petrakis, G.S. Armatas, Development of enhanced surface area LaFeO3 perovskites using amino acids as templating agents, Mater. Res. Bull. 83 (2016) 491–501, https://doi.org/10.1016/j.materresbull.2016.06.034.

[38] Z. Bian, Z. Wang, B. Jiang, P. Hongmanorom, W. Zhong, S. Kawi, A review on perovskite catalysts for reforming of methane to hydrogen production, Renew. Sustain. Energy Rev. 134 (2020), https://doi.org/10.1016/j.rser.2020.110291.

[39] M. Pinzón, A. Sánchez-Sánchez, A. Romero, A.R. de la Osa, P. Sánchez, Self-combustion Ni and Co-based perovskites as catalyst precursors for ammonia decomposition. Effect of Ce and Mg doping, Fuel 323 (2022), https://doi.org/10.1016/j.fuel.2022.124384.

[40] J. Kubo, W. Ueda, Catalytic behavior of AMoOx (A = Ba, Sr) in oxidation of 2-propanol, Mater. Res. Bull. 44 (2009) 906–912, https://doi.org/10.1016/j.materresbull.2008.08.013.

[41] M.S.P. Sudhakaran, M.M. Hossain, G. Gnanasekaran, Y.S. Mok, Dry reforming of propane over γ-Al2O3 and nickel foam supported novel SrNiO3 perovskite catalyst, Catalysts 9 (2019), https://doi.org/10.3390/catal9010068.

[42] N. Ahmad, F. Alharthi, M. Alam, R. Wahab, S. Manoharadas, B. Alrayes, Syngas production via co2 reforming of methane over srnio3 and cenio3 perovskites, Energies 14 (2021), https://doi.org/10.3390/en14102928.

[43] A. Kumar, A.S. Verma, S.R. Bhardwaj, Prediction of Formability in Perovskite-type Oxides, 2008.

[44] W. Li, D. Li, X. Gao, A. Gurlo, S. Zander, P. Jones, A. Navrotsky, J.Z. Shen, R. Riedel, E. Ionescu, D. Trans, W. Li, D. Li, X. Gao, A. Gurlo, S. Zander, P. Jones, A. Navrotsky, Z. Shen, R. Riedel, E. Ionescu, Study on the thermal conversion of scheelite-type ABO 4 into perovskite-type AB(O,N) 3, (n.d.). https://doi.org/10.1039/c0xx00000x..

[45] L. Wang, Z. Yang, X. Yin, S.D. Taylor, X. He, C. Sin Tang, M.E. Bowden, J. Zhao, J. Wang, J. Liu, D.E. Perea, L. Wangoh, A.T. S Wee, H. Zhou, S.A. Chambers, Y. Du, Spontaneous Phase Segregation of Sr 2 NiO 3 and SrNi 2 O 3 during SrNiO 3 Heteroepitaxy, 2021.

[46] S. Wang, M. Mohammadi, I. Dirba, K. Hofmann, B. Albert, L. Alff, P. Komissinskiy, L. Molina-Luna, Molecular dynamics simulation of crystal structure and heat capacity in perovskite-type molybdates SrMoO3 and BaMoO3, Comput. Mater. Sci. 197 (2021), https://doi.org/10.1016/j.commatsci.2021.110609.

[47] Y.F. Liu, S.H. Dai, Y.N. Lu, H.H. Min, Microwave heating synthesis and luminescence property of Eu 3+ doped SrMoO 4 micro-octahedrons, Powder Technol. 221 (2012) 412–418, https://doi.org/10.1016/j.powtec.2012.01.039.

[48] C.B. Njoku, R.J. Kriek, Application of Sm0.8Sr0.2Fe1-xCoxO3-δ (x = 0.2, 0.5, 0.8) perovskite for the oxygen evolution reaction in alkaline media, Electrocatalysis 10 (2019) 305–313, https://doi.org/10.1007/s12678-018-0498-7.

[49] A. Radetinac, J. Ziegler, M. Vafaee, L. Alff, P. Komissinskiy, Growth and interface engineering in thin-film Ba0.6Sr0.4TiO3/SrMoO3 heterostructures, J. Cryst. Growth 463 (2017) 134–138, https://doi.org/10.1016/j.jcrysgro.2017.02.015.

[50] P. Salg, D. Walk, L. Zeinar, A. Radetinac, L. Molina-Luna, A. Zintler, R. Jakoby, H. Maune, P. Komissinskiy, L. Alff, Atomically interface engineered micrometer-thick SrMoO3 oxide electrodes for thin-film BaxSr1- xTiO3 ferroelectric varactors tunable at low voltages, Apl. Mater. 7 (2019), https://doi.org/10.1063/1.5094855.

[51] Q.H. Wu, M. Liu, W. Jaegermann, X-ray photoelectron spectroscopy of La0.5Sr 0.5MnO3, Mater. Lett. 59 (2005) 1980–1983, https://doi.org/10.1016/j.matlet.2005.01.038.

[52] H.W. Nesbitt, D. Legrand, G.M. Bancroft, Interpretation of Ni2p XPS Spectra of Ni Conductors and Ni Insulators, n.d..

[53] M.F. Al-Kuhaili, S.H.A. Ahmad, S.M.A. Durrani, M.M. Faiz, A. Ul-Hamid, Application of nickel oxide thin films in NiO/Ag multilayer energy-efficient coatings, Mater. Sci. Semicond. Process. 39 (2015) 84–89, https://doi.org/10.1016/j.mssp.2015.04.049.

[54] S. Bewana, M. Joe Ndolomingo, R. Meijboom, N. Bingwa, Cobalt oxide promoted tin oxide catalysts for highly selective glycerol acetalization reaction, Inorg. Chem. Commun. 128 (2021), https://doi.org/10.1016/j.inoche.2021.108578.

[55] M.I. Shukoor, H.A. Therese, L. Gorgishvili, G. Glasser, U. Kolb, W. Tremel, From layered molybdic acid to lower-dimensional nanostructures by intercalation of amines under ambient conditions, Chem. Mater. 18 (2006) 2144–2151, https://doi.org/10.1021/cm051685a.

[56] Q. Xia, H. Zhao, Z. Du, Z. Zeng, C. Gao, Z. Zhang, X. Du, A. Kulka, K.-wierczek, Facile synthesis of MoO3/carbon nanobelts as high-performance anode material for lithium ion batteries, Electrochim. Acta 180 (2015) 947–956, https://doi.org/10.1016/j.electacta.2015.09.042.

[57] Y. Li, Y. Zheng, J. Yao, J. Xiao, J. Yang, S. Xiao, Facile synthesis of nanocrystalline-assembled nest-like NiO hollow microspheres with superior lithium storage performance, RSC Adv. 7 (2017) 31287–31297, https://doi.org/10.1039/c7ra05373h.

[58] H.Q. Wang, X.P. Fan, X.H. Zhang, Y.G. Huang, Q. Wu, Q.C. Pan, Q.Y. Li, In situ growth of NiO nanoparticles on carbon paper as a cathode for rechargeable Li-O2 batteries, RSC Adv. 7 (2017) 23328–23333, https://doi.org/10.1039/c7ra02932b.

[59] G. Cainelli, P. Galletti, D. Giacomini, P. Orioli, Solvent and Temperature Effect in Aldol Condensation between the Lithium Enolate of Tert-Butyl Acetate and 2-phenyl Propanal: Enthalpy and Entropy Contribution, 2001.

[60] M.T. Casale, A.R. Richman, M.J. Elrod, R.M. Garland, M.R. Beaver, M.A. Tolbert, Kinetics of acid-catalyzed aldol condensation reactions of aliphatic aldehydes, Atmos. Environ. 41 (2007) 6212–6224, https://doi.org/10.1016/j.atmosenv.2007.04.002.

[61] A. Parejas, D. Cosano, J. Hidalgo-Carrillo, J.R. Ruiz, A. Marinas, C. Jiménez-Sanchidrián, F.J. Urbano, Aldol condensation of furfural with acetone over Mg/Al mixed oxides. Influence of water and synthesis method, Catalysts 9 (2019), https://doi.org/10.3390/catal9020203.

[62] D. Liang, G. Li, Y. Liu, J. Wu, X. Zhang, Controllable self-aldol condensation of cyclopentanone over MgO-ZrO2 mixed oxides: origin of activity & selectivity, Catal. Commun. 81 (2016) 33–36, https://doi.org/10.1016/j.catcom.2016.04.008.

[63] W.B. Chen, Y.H. Liao, X.L. Du, X.M. Zhang, W.C. Yuan, Catalyst-free aldol condensation of ketones and isatins under mild reaction conditions in DMF with molecular sieves 4 Å as additive, Green Chem. 11 (2009) 1465–1476, https://doi.org/10.1039/b906684e.

[64] G. Mitran, S. Chen, D.K. Seo, Molybdenum dopped copper ferrites as active catalysts for alcohols oxidative coupling, Materials 12 (2019), https://doi.org/10.3390/ma12111871.

[65] J. Liu, K. Wu, Z. Li, W. Li, Y. Ning, W. Wang, Y. Yang, Preparation of bimetal Co–Ni supported on Mg–Al oxide for chemocatalytic upgrading of tailored fermentation products to energy intensive fuels, Green Energy Environ. 7 (2022) 457–466, https://doi.org/10.1016/j.gee.2020.10.011.

[66] J. Chen, M. Xu, S. Yu, Y. Xia, S. Lee, Nickel-Catalyzed claisen condensation reaction between two different amides, Org. Lett. 22 (2020) 2287–2292, https://doi.org/10.1021/acs.orglett.0c00485.

[67] P. Bernard, P. Stelmachowski, P. Broś, W. Makowski, A. Kotarba, Demonstration of the influence of specific surface area on reaction rate in heterogeneous catalysis, J Chem Educ 98 (2021) 935–940, https://doi.org/10.1021/acs.jchemed.0c01101.

[68] S. Bewana, M.J. Ndolomingo, E. Carleschi, B.P. Doyle, R. Meijboom, N. Bingwa, Inorganic perovskite-induced synergy on highly selective Pd-catalyzed hydrogenation of cinnamaldehyde, ACS Appl. Mater. Interfaces 11 (2019) 32994–33005, https://doi.org/10.1021/acsami.9b10820.

[69] E.C. Lima, A.A. Gomes, H.N. Tran, Comparison of the nonlinear and linear forms of the van't Hoff equation for calculation of adsorption thermodynamic parameters (ΔS° and ΔH°), J. Mol. Liq. 311 (2020), https://doi.org/10.1016/j.molliq.2020.113315.

[70] C. Capello, U. Fischer, K. Hungerbühler, What is a green solvent? A comprehensive framework for the environmental assessment of solvents, Green Chem. 9 (2007) 927–993, https://doi.org/10.1039/b617536h.

[71] G. Guillena, M. del Carmen Hita, C. Nájera, BINAM-prolinamides as recoverable catalysts in the direct aldol condensation, Tetrahedron Asymmetry 17 (2006) 729–733, https://doi.org/10.1016/j.tetasy.2006.02.004.

[72] R. Mestres, A green look at the aldol reaction, Green Chem. 6 (2004) 583–603, https://doi.org/10.1039/b409143b.

[73] T. Kano, J. Takai, O. Tokuda, K. Maruoka, Design of an axially chiral amino acid with a binaphthyl backbone as an organocatalyst for a direct asymmetric aldol reaction, Angewandte Chemie - International Edition 44 (2005) 3055–3057, https://doi.org/10.1002/anie.200500408.

[74] P.S. Samudrala, A.V. Nakhate, S.S.R. Gupta, K.B. Rasal, G.P. Deshmukh, C.R. Gadipelly, S. Theegala, D.K. Dumbre, S. Periasamy, V.R.C. Komandur, S. K. Bhargava, L.K. Mannepalli, Oxidative coupling of carboxylic acids or benzaldehydes with DMF using hydrotalcite-derived oxide catalysts, Appl. Catal., B 240 (2019) 348–357, https://doi.org/10.1016/j.apcatb.2017.12.058.

[75] M.M. Heravi, M. Ghavidel, L. Mohammadkhani, Beyond a solvent: triple roles of dimethylformamide in organic chemistry, RSC Adv. 8 (2018) 27832–27862, https://doi.org/10.1039/c8ra04985h.

[76] W. Liu, C. Chen, H. Liu, Dimethylamine as the key intermediate generated in situ from dimethylformamide (DMF) for the synthesis of thioamides, Beilstein J. Org. Chem. 11 (2015) 1721–1726, https://doi.org/10.3762/bjoc.11.187.

[77] J.I. Di Cosimo, V.K. Díez, C. Ferretti, C.R. Apesteguía, Basic catalysis on MgO: generation, characterization and catalytic properties of active sites, Catalysis 26 (2014) 1–28, https://doi.org/10.1039/9781782620037-00001.